Eur. Phys. J. D **22**, 193–198 (2003)
DOI: 10.1140/epjd/e2002-00242-8

THE EUROPEAN PHYSICAL JOURNAL D

High resolution laser spectroscopy of NaAr: Improved interaction potential for the X $^2\Sigma^+$ ground state

D. Schwarzhans[a] and D. Zimmermann[b]

Technische Universität Berlin, Institut für Atomare Physik und Fachdidaktik, Hardenbergstr. 36, 10623 Berlin, Germany

Received 28 August 2002 / Received in final form 15 October 2002
Published online 17 December 2002 –

Abstract. The absorption spectrum of NaAr has been investigated with high resolution using a supersonic beam of molecules and a tunable dye laser. About 3 300 absorption lines due to the transition $A\,^2\Pi \leftarrow X$ and $B\,^2\Sigma \leftarrow X$ have been observed. In addition, we observed the spectral distribution of the fluorescence for a particular absorption line. From all experimental data the $X\,^2\Sigma^+$ interaction potential has been deduced in a fully quantum–mechanical method of approach. The potential is given in terms of an analytical Hartree-Fock-Dispersion function. For the equilibrium parameters of the X state we get $R_e = 5.01(1)$ Å and $D_e = 41.6(2)$ cm^{-1}.

PACS. 33.20.Kf Visible spectra – 33.20.Vq Vibration-rotation analysis

1 Introduction

The $X\,^2\Sigma^+$ interaction potential of NaAr has been the subject of numerous investigations, both experimentally and theoretically, for a long time. Renewed interest in accurate information on this potential comes *e.g.* from differential optical collisions [1] or from experiments measuring the index of refraction of an atomic matter wave passing through a dilute medium of rare gas atoms [2]. As is well-known, high-resolution laser spectroscopy is a suitable experimental tool for a precise determination of the energy values of the rovibrational levels. The bound part of the interatomic potential can be derived from the observed energy levels and will be particularly accurate if all bound rovibrational levels are included. The energy values of the rovibrational levels of the X state are deduced from the absorption lines which are due to the transitions $A\,^2\Pi \leftarrow X\,^2\Sigma$ and $B\,^2\Sigma \leftarrow X\,^2\Sigma$. These transitions lead to the first excited states $A\,^2\Pi$ and $B\,^2\Sigma$ which both correlate with the first excited $3\,^2$P state of the Na atom in the limit of dissociation.

In addition, the spectral distribution of the fluorescence $A \rightarrow X$ may be recorded after populating selectively a certain rovibrational level of the A-state by means of laser excitation. As the equilibrium distance of $A\,^2\Pi$ is much lower compared with $X\,^2\Sigma$, part of the fluorescence is due to bound-free transitions leading to the repulsive branch of the X potential and allowing a determination of this branch.

A first laserspectroscopic determination of the X potential of NaAr has been performed a long time ago by Tellinghuisen *et al.* [3]. The experimental data consisted of the energy values of vibrational levels $v'' = 0$–4 and of the spectral distributions of fluorescence for two selectively populated sublevels of the $A\,^2\Pi$ state. The X potential was given in form of a modified Morse function. However, the semiclassical RKR method and the semiclassical long-range theory were used for inversion of the vibrational levels to the bound part of the potential. In addition, the energy values of vibrational levels $v'' = 2, 3$, and 4 were deduced from bound-bound transitions of fluorescence, the experimental error being distinctly larger compared with the error of the high-resolution data for $v'' = 0$ and 1. In a second laserspectroscopic investigation performed by our group [4] highly accurate values of the parameters of molecular vibration and rotation have been obtained for $v'' = 0$–4, but no efforts were undertaken to deduce the $X\,^2\Sigma^+$ potential.

The aim of the present work was: (i) to get accurate energy values for all bound rovibrational levels, (ii) to measure the spectral distribution of fluorescence and (iii) to deduce the X potential in form of an analytical function from all these data using a fully quantum mechanical method of approach. All items of this program have successfully been worked out. In particular, two additional vibrational levels $v'' = 5$ and 6 could be observed for the first time, the latter being only about 0.07 cm^{-1} below the limit of dissociation. Our improved $X\,^2\Sigma^+$ potential covers the complete bound part, whereas the repulsive part could be determined for energies up to 2 200 cm^{-1}.

Our paper is organized as follows: Section 2 presents the experimental details and the spectroscopic results,

[a] *Now at* Knick Elektronische Messgeräte, Beuckestr. 22, 14163 Berlin, Germany.
[b] e-mail: dz@kalium.physik.tu-berlin.de

whereas the derivation of the $X\ ^2\Sigma^+$ potential is described in Section 3. The paper closes with a summary in Section 4.

2 Experimental procedure and spectroscopic results

The experimental arrangement was quite similar to that used in our previous investigation of higher excited electronic states of KAr [5], where a schematic diagram of the apparatus can be found. Only substantial changes – being required in going from KAr to NaAr – will be mentioned in the following. The molecules were produced by supersonic expansion of a mixture of Na vapor and pure argon gas into a vacuum through a nozzle. In our previous work the nozzle was provided by a small molybdenum plate with a central hole taken from electron microscopy and being attached to the nozzle holder by a rolling procedure. This pressure sealing became more and more leaky, in particular after a change in the surface properties of the molybdenum plate by the manufacturer. Therefore, a new type of nozzle had to be developed. The nozzle including the nozzle holder was built from a full block of stainless steel. The nozzle channel of 4 mm diameter was predrilled in our machine shop up to a distance of about 0.5 mm beyond breakthrough. The nozzle hole with a diameter of typically 0.1 mm was then manufactured by a company offering high-precision drilling of small holes into thin metal walls. With this design clogging could largely be avoided.

The remaining oven assembly was the same as in our investigation of LiAr [6], where more details can be found. Typical operating conditions for NaAr are: temperature of the Na supply 420° C, temperature of the nozzle and the gas inlet 450 °C, Ar pressure 6×10^5 Pa, pressure in the vacuum chamber 0.3–0.8 Pa. With these parameters the molecular beam could usually be run in a stable manner for several hours.

The molecular beam was crossed by a laser beam about 5 mm downstream from the nozzle. The laser was a commercial cw ring dye laser system (Coherent 699-21) with Rhodamin 6 G as a dye and pumped by a 20 W argon-ion laser (Coherent Innova 100). The dye laser could be scanned over a range of 1 cm^{-1}. The total laser-induced fluorescence was observed in the direction perpendicular to both the laser and the molecular beam by means of a photomultiplier.

The absorption spectrum of NaAr was recorded between 16 734 and 17 008 cm^{-1} in sections of 1 cm^{-1} with an overlap between subsequent scans of 0.1–0.3 cm^{-1}. A relative wavenumber scale was provided by the transmission peaks of a confocal, temperature-stabilized Fabry-Perot-Interfermometer (FPI) whose free spectral range has been determined with a relative accuracy of 1×10^{-6}. Absolute wavenumbers were obtained by recording the absorption spectrum of iodine in a cell. In order to get a continuous absorption spectrum the different sections were connected by means of the overlap with the help of a home-made computer program SCANCON. A small misalignment of the angle between laser and atomic beam from 90° leads to a small Doppler shift of the NaAr absorption lines which is different, in particular for runs on different days. Therefore, the Doppler shift has been measured after each realigning of the oven assembly by taking data for counterpropagating laser beams. In addition, the weak non-linearity of the wavenumber scale and a tiny residual drift of the FPI markers have properly been taken into account.

Most scans have been recorded with a laser power of 30 mW corresponding to a power density of about 3 W/cm^2 leading to a considerable contribution of saturation to the line width at least for the most intense vibrational bands.

The assignment of quantum numbers to the observed absorption lines was rather straightforward within the range of wavenumbers covered in previous investigations [3,4,7]. In the region outside of these wavenumbers assignment was possible by a simple extrapolation of the spectroscopic parameters. For the $A\ ^2\Pi$ state our data now extend over vibrational levels $v' = 5$–12, 17, 18 compared with $v' = 7$–10 in the previous work. The analysis of our data was impeded by the occurrence of local perturbations in the $A\ ^2\Pi$ state which have not been taken into account in the previous work. We have successfully performed a full deperturbation analysis. In addition, we obtained first spectroscopic results for the $B\ ^2\Sigma$ states for vibrational levels $v' = 3$–5, but the results which concern the two excited states $A\ ^2\Pi$ and $B\ ^2\Sigma$ will be presented in a separate paper [8].

With respect to the molecular ground state $X\ ^2\Sigma$ we have observed the vibrational levels $v'' = 5$ and 6 for the first time in the present work. In Figure 1 we have depicted a section of the absorption spectrum of NaAr showing vibrational bands with lower level $v'' = 5$. As is well known from previous work [7], the absorption lines of NaAr appear in pairs of lines separated by the molecular hyperfinestructure (hfs) splitting, which is equal to the atomic hfs splitting of the $3s\ ^2$S level of the sodium atom of 0.059 cm^{-1} for all lines in a coupling case b_β. The observed absorption lines of NaAr were fitted to a Gaussian lineshape, and up to ten different Gaussians were used in regions of strong overlapping. The accuracy of the center wavenumber of a line was estimated to be $\pm$ 0.001 cm^{-1} on the relative scale and $\pm$ 0.003 cm^{-1} on the absolute scale, the latter error being mainly due to the limited accuracy of the iodine absorption lines [9].

The center wavenumbers were fitted to expressions for the energy difference between the upper and lower level. The energy values in the $X\ ^2\Sigma^+$ state are given by the well-known formula [10]

$$E(v,N) = T_v + B_v\,N(N+1) - D_v\,[N(N+1)]^2 + H_v[N(N+1)]^3 \quad (1)$$

where N is the rotational quantum number. Spin-rotation splitting was below resolution of our apparatus and, therefore, was neglected. The energy values of the levels of the $A\ ^2\Pi$ state were obtained by diagonalization of a 2×2 matrix which was set up in a case a basis with $\Omega = 1/2$ and $\Omega = 3/2$. The matrix elements are given as

Table 1. Spectroscopic parameters (in cm^{-1}) of $X\ ^2\Sigma^+$ ground state of NaAr: N_{max} highest observed bound rotational level (highest observed quasibound level in parenthesis), n number of observed absorption lines. Errors in the last digit are quoted in parenthesis and represent three times the standard deviation of the fit. Values marked by an asterisk have been held fixed during the fit. p: present work.

v''	T	10^2B	10^6D	$10^{10}H$	N_{max}	n	Ref.
0	0*	4.437(2)	2.51(5)	−1.9(5)	28	934	p
		4.432(2)	2.30(4)	−4.3(4)		715	4
		4.444(2)	2.56(7)	–			7
1	11.243(1)	4.056(2)	3.11(7)	−6.1(8)	24	734	p
	11.243(2)	4.051(2)	2.88(6)	−9.0(7)		397	4
	11.244(14)	4.059(7)	2.77(72)	–			7
2	20.311(1)	3.604(2)	3.35(8)	−28.5(9)	20(23)	665	p
	20.308(5)	3.608(3)	3.70(14)	−22(2)		299	4
	20.290(200)	–	–	–			3, 7
3	27.137(1)	3.081(3)	4.4(2)	−81(4)	16(17)	518	p
	27.134(8)	3.086(4)	5.2(4)	−60(7)		131	4
	26.710(450)	–	–	–			3, 7
4	31.722(2)	2.446(7)	5.8(8)	−300(30)	11(12)	275	p
	31.720(13)	2.452(20)	8 (2)	−220(50)		51	4
	31.180(600)	–	–	–			3, 7
5	34.219(2)	1.69(2)	10(6)	−1500(500)	7	171	p
6	35.086(4)	0.52(3)	0*	0*	2	14	p

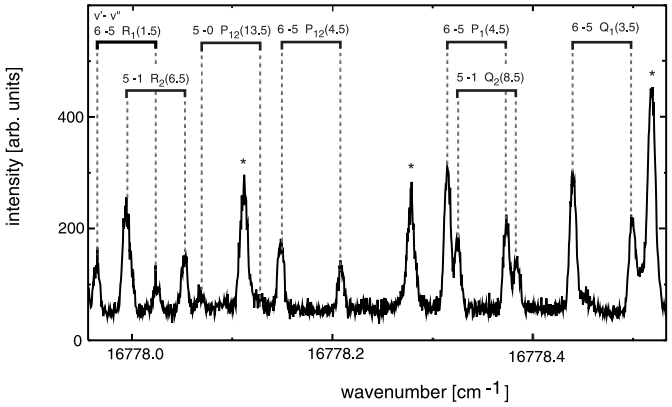

Fig. 1. Section of the absorption spectrum of NaAr due to the electronic transition $A\ ^2\Pi_\Omega \leftarrow X\ ^2\Sigma^+$ with vibrational assignment in the form $v' - v''$. The upper and lower row correspond to $\Omega = 1/2$ and 3/2, respectively. Rotational assignment is defined in reference [11]. The 3 lines marked by an asterisk are unassigned and most probably due to Na_2.

equations (2–4) in reference [11]. The non-diagonal matrix element between $\Omega = 1/2$ and $\Omega = 3/2$ takes account of the effect of spin-uncoupling in the $A\ ^2\Pi$ state.

Altogether, 3 311 absorption lines were included in a global least-squares fit procedure yielding the spectroscopic parameters of all vibrational levels separately and reproducing the input data with a mean deviation of 0.002 cm^{-1}. The range of vibrational levels covered by this global fit is $v'' = 0$–6 for $X\ ^2\Sigma$, $v' = 5$–11, 17, 18 for $A\ ^2\Pi_{1/2}$, and $v' = 5$–10, 12 for $A\ ^2\Pi_{3/2}$. Absorption lines leading to the vibrational level $v' = 12$ of $A\ ^2\Pi_{1/2}$ or $v' = 11$ of $A\ ^2\Pi_{3/2}$ have been excluded from the determination of the $X\ ^2\Sigma$ spectroscopic parameters in order to avoid any effect of an imperfect treatment of the local perturbation between these two vibrational levels on the parameters of the ground state. The results of the $A\ ^2\Pi$ spectroscopic parameters will be published in a separate paper [8], but are already available from Table 5.4 of reference [12]. Similar reasons apply for the exclusion of all $B \leftarrow X$ absorption lines from the global fit. A complete listing of experimental data and fit results for all 3 311 absorption lines observed in the present work is given in a separate report [13] and is available from the authors on request.

Table 1 shows our values for the spectroscopic parameters of the NaAr – $X\ ^2\Sigma^+$ state in comparison with previous results. The values of T_v and B_v from different sources agree quite well within limits of error. Some discrepancies are present for the parameters D_v and H_v of centrifugal distortion and might be caused by different small imperfections of the molecular Hamiltonian leading to a considerable change of small quantities like D_v and H_v. However, due to the exclusion of all problematic lines from the fit procedure our present results should be more reliable than the previous ones. In addition, they are distinctly more accurate.

N_{max} in Table 1 is the rotational quantum number of the highest rovibrational level being observed. Some of these levels are above the limit of dissociation of the X state and are quasibound due to the effect of the rotational barrier $Z(R) = \hbar^2\, N(N+1)/2\mu\ R^2$ where μ is the reduced mass. Absorption lines with a quasibound lower level are discernible in the spectrum due to their increased

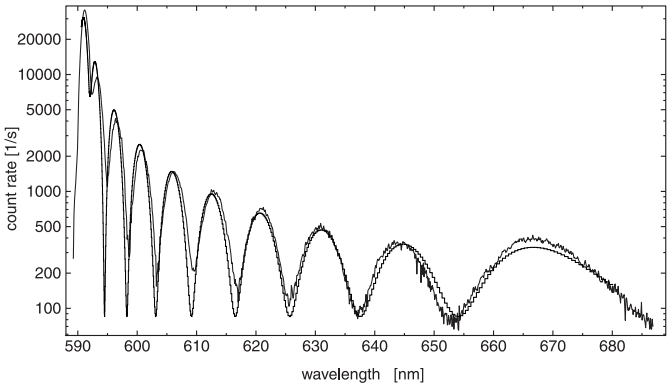

Fig. 2. Spectral distribution of fluorescence starting from the f level with $v' = 9$, $J' = 10.5$ of the $A\,^2\Pi_{3/2}$ state. The dashed line is the result of the calculation using our best potential. The units of intensity are proportional to counts per second and nanometer.

intensity (in combination with a decreased linewidth). The latter effect is caused by saturation: all absorption lines are saturated in our case. If the lifetime of the lower state is decreased due to tunneling through the rotational barrier, the corresponding absorption line is less saturated and, therefore, appears with higher intensity and decreased linewidth in the spectrum. Line broadening due to tunnelling can be observed, if the lifetime becomes short enough in order to exceed the linewidth due to saturation. These quasibound levels have been included in the determination of the spectroscopic parameters and in the derivation of the $X\,^2\Sigma^+$ interaction potential.

A second source of experimental information on the $X\,^2\Sigma$ interaction potential comes from the observed spectral distribution of the fluorescence after populating selectively a certain rovibrational level of the $A\,^2\Pi$ state. Figure 2 shows our experimental result for selective excitation of the f level with $v' = 9$, $J' = 10.5$ of $A\,^2\Pi_{3/2}$. The laser was tuned to the R_f (9.5) line of the vibrational transition $v' = 9 \leftarrow v'' = 0$ at 16 921.464 cm^{-1} corresponding to a wavelength of 590.97 nm. A grating monochromator (Jobin-Yvon HR 320) being placed into the beam of the fluorescent light was scanned. The experimental curve has been corrected for the spectral response of the detection device (monochromator plus photomultiplier) which has been measured separately using a tungsten band lamp.

The experimental curve in Figure 2 shows a clear "reflection" structure reflecting the vibrational wavefunction of the upper level *via* the Mulliken difference potential into the observed spectrum [14]. There exist 10 maxima corroborating the assignment $v' = 9$ to the upper level. All bound-bound transitions $A\,^2\Pi_{3/2}\ v' = 9 \rightarrow X\,^2\Sigma\ v''$ are covered by the first maximum on the low wavelength side, whereas the remaining structure is due to bound-free transitions. The spectrum extends over a wavelength interval between 590 and 680 nm. Therefore, we obtain information on the repulsive part of the $X\,^2\Sigma^+$ interaction potential from 0 to 2 200 cm^{-1}, corresponding to R values between 2.5 and 4.2 Å.

3 Determination of interatomic potential

The $X\ ^2\Sigma^+$ interatomic potential was determined in a fully quantum-mechanical approach solving the Schrödinger equation of nuclear motion numerically using an effective potential $V(R) = U(R) + Z(R)$ where $Z(R)$ is the contribution of molecular rotation already given in Section 2. $U(R)$ was provided in form of an analytical function with a certain number of free parameters, *e.g.* a Hartree-Fock-Dispersion (HFD)-function. The calculated energy values were compared with the experimental energies, and the parameters of the potential were varied within a standard fit routine until the deviation was minimal. More details on this method of approach are given in our previous work [11,15,16].

Our input data consisted of the energies of altogether 120 rovibrational levels including 5 quasibound levels. These energies were obtained by using the parameters of Table 1 together with equation (1). The number $N_{\max} + 1$ of rotational levels can be deduced from Table 1 for each vibrational level. As all bound levels have been observed, our input data represent the most complete set for an accurate determination of the bound part of the $X\,^2\Sigma$ potential. In addition, the wavelength values of the 8 maxima of the dispersed fluorescence I_λ on the high wavelength side have been included into the fit using the same potential function and calculating I_λ according to equation (13) in reference [15].

Several analytical functions have been tried, *e.g.* HFD, Tang-Toennies (T-T), Morse-van der Waals (MVW) (see Ref. [11] for definition) and Thakkar (Th) [17]. Our best result was obtained using a HFD function which is given by

$$U(R) = A\mathrm{e}^{-\alpha R+\beta R^2} - \left(\frac{C_6}{R^6} + \frac{C_8}{R^8} + \frac{C_{10}}{R^{10}} + \frac{C_{12}}{R^{12}} \right) F(R)$$

$$F(R) = \begin{cases} 1 & R \geq R_m \\ \text{for} & \\ \exp\ [-(R_m/R - 1)^2] & R < R_m \end{cases} \qquad (2)$$

$F(R)$ is a damping function cutting down the well-known long-range power series expansion for small values of R. Compared with previous work an additional term C_{12}/R^{12} was required in order to reproduce the level $v'' = 6$ as a bound state. The HFD function was the only expression being flexible enough to represent the bound and the repulsive part by one single function.

The parameters of our best potential are compiled in Table 2. By means of this potential the 120 discrete energy levels and the 8 wavelength values corresponding to the maxima of I_λ are well reproduced with a standard deviation of 3.6×10^{-3} cm^{-1} and 0.47 nm, respectively, which is close to the experimental error. As can be seen from Figure 2, the calculated curve of I_λ is in accordance with the experimental curve, not only near the maxima, but also with respect to the wavelength positions of the minima and even with respect to intensities, in particular on the high wavelength part of the spectrum. The residuals between calculation and experiment of the wavelength

Table 2. Parameters of HFD function for $X\ ^2\Sigma^+$ interatomic potential of NaAr. A higher number of digits is given in order to allow an accurate recalculation. The van der Waals coefficients in the right column are the result of a theoretical calculation [22].

$10^{-4}\ A$ [cm^{-1}]	6.2064 7852	
α [$\mathrm{Å}^{-1}$]	0.8420 8509	
β [$\mathrm{Å}^{-2}$]	−0.1313 6826	
R_m [Å]	7.9107 8777	
$10^{-5}\ C_6$ [cm^{-1} $\mathrm{Å}^6$]	7.0362 0968	9.09
$10^{-7}\ C_8$ [cm^{-1} $\mathrm{Å}^8$]	5.0206 3345	1.43
$10^{-9}\ C_{10}$ [cm^{-1} $\mathrm{Å}^{10}$]	−1.0693 3342	0.294
$10^{-10}\ C_{12}$ [cm^{-1} $\mathrm{Å}^{12}$]	1.0422 1876	–
R_e [Å]	5.00638	
D_o [cm^{-1}]	35.1539	
D_e [cm^{-1}]	41.5592	

values of the maxima of I_λ allow an estimate of the accuracy of the repulsive part of $U(R)$, which turns out to be $\pm$ 15 cm^{-1} in our case. Another contribution to the error of $U(R)$ might be caused by a probable R-dependence of the electronic transition dipole element μ ($X \leftarrow A$). According to a theoretical calculation [18] $\mu(R)$ varies by about 1.5% between R = 3 and 5 Å, thus allowing to neglect this effect in our present work.

A closer inspection of Figure 2 shows slight deviations of opposite sign between experiment and calculation in the low- and high-wavelength part. This observation indicates a possible improvement of the fit by slightly shifting $U(R)$ to higher values for $0 \le U(R) \le 850$ cm^{-1} and to lower value on the high-wavelength side. Unfortunately, we found no modification of the HFD or another function which could meet these requirements.

For the bound part of $U(R)$ an estimate of the accuracy might be obtained by comparing the values of the potential using different analytical functions and applying the same fit procedure as before. For MVW we get a fit of similar quality as for HFD, whereas T-T or Th lead to an increase in the standard deviation by a factor of 5–10. Nevertheless, even the results of these functions are covered by a margin of $\pm$ 0.1 cm^{-1} which we consider as our error estimate for the major part of the bound region of the $X\ ^2\Sigma^+$ interatomic potential. Only near the minimum the error is slightly larger due to extrapolation and is estimated to be $\pm$ 0.2 cm^{-1}.

It is sometimes preferable to shift the zero of the energy from the lowest rovibrational level $v'' = N'' = 0$ to the dissociation limit of $X\ ^2\Sigma^+$. Therefore, an accurate value of the dissociation energy D_o is required. From our best potential we deduce a value of D_o = 35.15(7) cm^{-1} as our final result, where the error margins again cover the results of the fits with all other functions. For equilibrium distance R_e and well-depth D_e we get from our best potential R_e = 5.01(1) Å, D_e = 41.6(2) cm^{-1}.

Finally, our best potential will be compared with recent results of other investigations, both experimentally and theoretically. Figure 3 (upper panel) shows our experimental potential together with the result of a recent *ab initio* calculation by Czuchaj [19]. Considerable differences of the order of 100 cm^{-1} occur with respect to our results, in particular for 3 Å $\le R \le$ 4.5 Å. The quantum chemical potential of Kerner and Meyer [20], based on the introduction of core polarisation potentials for the rare gas atom, is in almost perfect agreement with our potential. Therefore, we have depicted the difference between both potentials in the lower panel of Figure 3. The same kind of representation was used for the model potential of Düren *et al.* [21] and the experimental potential of Tellinghuisen *et al.* [3]. All three potentials are in agreement with our result within the error margins for $R >$ 4 Å, but show some deviations outside error limits between 2.5 and 4 Å.

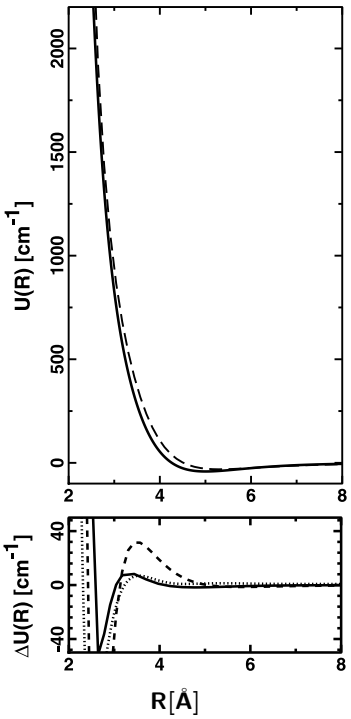

Fig. 3. Upper panel: the $X\ ^2\Sigma^+$ interaction potential of NaAr, present work (full line), Czuchaj [19] (dashed line). Lower panel: difference between Kerner-Mayer [20] (full line), Düren *et al.* [21] (dashed line) and Tellinghuisen *et al.* [3] (dotted line) and our result.

Figure 4 is an enlarged view of the bound part of the $X\ ^2\Sigma^+$ potential. In this expanded scale one recognizes small deviations of the order of a few cm^{-1} between our result and the Kerner-Mayer potential near the minimum which are distinctly larger than our error estimates for this region. Deviations of the order of 10 cm^{-1} occur with respect to the *ab initio* potential of Czuchaj [19], whereas the model potential of Düren [21] is in almost perfect agreement with our experimental potential, at least around the minimum. As expected, the experimental potential of Tellinghuisen *et al.* [3] is close to ours, but shows small deviations outside limits of error.

In addition, we have depicted in Figure 4 the 7 bound vibrational levels $v'' =$ 0–6 as obtained experimentally

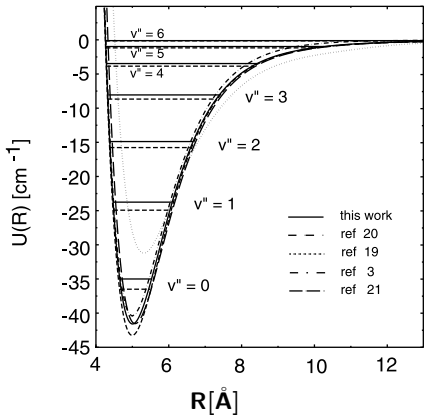

Fig. 4. The bound part of the $X\ ^2\Sigma^+$ interaction potential of NaAr. Experimental: present work and Tellinghuisen *et al.* [3], Theoretical: Czuchaj [19], Kerner-Mayer [20], Düren *et al.* [21].The vibrational levels $v'' = 0$–6 are indicated for the potential of the present work (full lines) and for Kerner-Mayer (dashed lines).

from high-resolution laser spectroscopy (full line) and calculated from the Kerner-Mayer potential (dashed line). The highest level $v'' = 6$ is bound by only 0.064 cm^{-1} and its wavefunction extends to about 15 Å, thus probing the $X\ ^2\Sigma^+$ interaction potential in the long-range limit.

A final remark refers to the coefficients C_6, C_8 of the long-range van der Waals interaction. These coefficients can be calculated quite reliably, and the results of different authors agree within a margin of 5–10%. As an example we have included into Table 2 the results of reference [22] which show only very qualitative agreement for C_6 and C_8. Our value of C_{10} even has the opposite sign. However, the long-range part of HFD is still of importance near the minimum. Therefore, these parameters must be considered as effective parameters having lost their original physical meaning.

4 Summary

We have determined the interaction potential of the ground state $X\ ^2\Sigma^+$ of the van der Waals molecule NaAr from high accuracy laserspectroscopic data using a fully quantum-mechanical approach. All bound rovibrational levels have been used as input data together with the wavelength values of the maxima of the spectral distribution of fluorescence. The accuracy of the potential was estimated to be ± 0.2 cm^{-1} and ± 15 cm^{-1} for the bound and the repulsive branch, respectively.

Our improved experimental potential corroborates the high quality of the quantum chemical calculation of Kerner and Mayer and the model potential of Düren *et al.* An independent experimental confirmation of the NaAr $X\ ^2\Sigma^+$ potential is provided by differential optical collisions between Na and Ar atoms [1,23]. The experimental results are almost completely reproduced by using the Kerner-Mayer potential. The accuracy of the repulsive part is estimated to be ± 10 cm^{-1} which is about the same as our estimate of ± 15 cm^{-1}. It would be interesting to use all available experimental data from spectroscopy and scattering as input data for a determination of an even more improved version of the $X\ ^2\Sigma^+$ interaction potential of NaAr.

The financial support of the Deutsche Forschungsgemeinschaft under contract No. ZI 186/5 is gratefully acknowledged.

References

1. J. Grosser, V. Hoffmann, F. Rebentrost, J. Phys. B **33**, L 577 (2000)
2. J. Vigué, Phys. Rev. A **52**, 3973 (1995)
3. J. Tellinghuisen, A. Ragone, M.S. Kim, D.J. Auerbach, R.E. Smalley, L. Wharton, D.H. Levy, J. Chem. Phys. **71**, 1283 (1979)
4. G. Aepfelbach, A. Nunnemann, D. Zimmermann, Chem. Phys. Lett. **96**, 311 (1983)
5. R. Michalak, D. Zimmermann, J. Mol. Spectr. **193**, 260 (1999)
6. R. Brühl, D. Zimmermann, Chem. Phys. Lett. **233**, 455 (1995)
7. R.E. Smalley, D.A. Auerbach, P.S.H. Fitch, D.H. Levy, L. Wharton, J. Chem. Phys. **66**, 3778 (1977)
8. D. Schwarzhans, D. Zimmermann, "Spectroscopy and interatomic potentials for the $A\ ^2\Pi$ and $B\ ^2\Sigma$ state of NaAr" in preparation
9. S. Gerstenkorn, P. Luc, *Atlas du spectre d'absorption de la molecule d'iode*, I–III (Éditions du CNRS, Paris, 1978)
10. G. Herzberg, *Molecular Spectra and Molecular Structure* (van Nostrand, Princeton, 1950), Vol. I
11. R. Brühl, D. Zimmermann, J. Chem. Phys. **114**, 3035 (2001)
12. D. Schwarzhans, Dissertation, Technische Universität Berlin, 2000, Internet address: `http://edocs.tu-berlin.de/diss/2000/schwarzhans_dirk.htm`
13. D. Schwarzhans, "Listing of analyzed spectral lines of NaAr", unpublished internal report, 2002, Internet adress: `http://iapf.physik.tu-berlin.de/DZ/Papers/Listing-NaAr-2002.pdf`
14. J. Tellinghuisen, Adv. Chem. Phys. **60**, 299 (1985)
15. R. Brühl, I. Kapetanakis, D. Zimmermann, J. Chem. Phys. **94**, 5865 (1991)
16. F. Bokelmann, D. Zimmermann, J. Chem. Phys. **104**, 923 (1996)
17. A.J. Thakkar, J. Chem. Phys. **62**, 1693 (1975)
18. E. Czuchaj, Z. Phys. A **292**, 109 (1979)
19. E. Czuchaj, private communication, Gdansk (Poland) July 2002
20. C. Kerner, Dissertation Universität Kaiserslautern, Germany, 1995
21. R. Düren, E. Hasselbrink, G. Moritz, Z. Phys. A **307**, 1 (1982); R. Düren, private communication, January 1983
22. T.R. Proctor, W.C. Stwalley, J. Chem. Phys. **66**, 2063 (1977)
23. J. Grosser, O. Hoffmann, F. Schulze Wischeler, F. Rebentrost, J. Chem. Phys. **111**, 2853 (1999)